Soil Dynamics and Earthquake Engineering 117 (2019) 47–57

Contents lists available at ScienceDirect

Soil Dynamics and Earthquake Engineering

journal homepage: www.elsevier.com/locate/soildyn

Study on dynamic fracture behavior of mode I crack under blasting loads

Ruifeng Liu, Zheming Zhu*, Meng Li, Bang Liu, Duanying Wan

MOE Key Laboratory of Deep Underground Science and Engineering, college of architecture and Environment, Sichuan University, 610065, China

ARTICLE INFO

Keywords:
Mode I crack
Blasting experiment
Crack initiation
Crack propagation
Crack propagation speed

ABSTRACT

Dynamic fracture behavior under impacting loads has been well studied, but for that under blasting loads, less attention has been paid. In order to investigate mode I crack propagation behavior of brittle materials under blasting, a new configuration specimen, i.e. single internal crack circular disc (SICCD) specimen was proposed in this paper, and it was applied in the blasting experiments. Crack propagation gauges (CPGs) were stuck along crack propagation paths to measure crack initiation and propagation time and crack propagation speeds. Green sandstone and PMMA were selected to make the SICCD specimens. Finite difference models were established by using AUTODYN code according to the SICCD specimen dimension and the loading curve measured near the borehole. Generally, the simulation results of crack propagation paths agree with the test results. Finite element code ABAQUS was applied in the calculation of dynamic stress intensity factors (SIFs), and the curves of dynamic SIFs versus time were obtained. By using these curves and the breaking time of the CPG wires, the mode I critical dynamic SIFs in initiation and in propagation were obtained. The results show that the measuring method of the critical dynamic SIFs of brittle materials under blasting presented in this paper is feasible and applicable. During crack propagations, the crack speed is not a constant, and the critical dynamic SIFs in propagation decreases with the increase of crack propagation speeds.

1. Introduction

As a traditional rock breaking method, fragmentation by explosive has the property of low cost and easy operation [1], and therefore, it is still a widely applied rock excavation method in mining, quarrying and tunneling. With increasing scale of such operations, proper designs of blasts and precise predictions of blasting results have become imperative in most operations. However, our understanding of the blasting process and the mechanism of blast-induced rock failure is only in the preliminary stage, as both the commercial explosives and the target rock are complex materials. The energy release characteristics in the former are highly variable, depending on the prevailing field parameters such as borehole diameter, density gradient, and sympathetic pressures from the detonation of neighbouring holes [2]. Similarly, the response of the target rock to high dynamic loading, which may last only for a few milliseconds, remains largely unknown.

Cracks exist widely in brittle materials, and under nearby blasting, the cracks may initiate and propagate [3], which may help to enhance rock fragmentation efficiency, but on the other hand, it may induce large geotechnical disasters, such as rockburst. Therefore, it is essential to implement the corresponding experimental and numerical study on crack propagation behavior under blasting, and the measuring method of the critical dynamic SIFs in initiation and in propagation of rock under blasting is one imperative task. This is because the critical dynamic SIFs is a threshold value which can be used to predict crack dynamic behavior so to predict cracked rock structure stability.

Currently, the study on rock dynamic fracture mainly focuses on impact loads, such as split Hopkinson pressure bar (SHPB) impacts and drop weight impacts, and many significant results have been achieved. With the development and improvement, the SHPB test system has been widely applied in the study of rock dynamic fracture [4–10]. However, the SHPB test system also has a disadvantage, i.e. the diameter of the pressure bar is not large enough, and therefore, for large size specimens, it is not suitable [11,12]. For small size specimens, the reflected tensile stress waves may reach crack tip to affect crack dynamic behavior during crack propagation [13]. Therefore, in dynamic experiments, the specimen size must be large enough so that as the reflected tensile stress wave from specimen boundary reaches crack tips, the crack dynamic activity have completed already.

In order to overcome the drawback of the small bar dimension of SHPB test system, a drop weight test system with large size impacting plate and transmission plate was designed which can be applied in the study of crack propagation behavior and fracture toughness of brittle materials with large size specimens, and based on this test system,

* Corresponding author.
E-mail address: zhuzheming@scu.edu.cn (Z. Zhu).

https://doi.org/10.1016/j.soildyn.2018.11.009
Received 18 June 2018; Received in revised form 14 October 2018; Accepted 13 November 2018

several papers were published [11,12,14,15,16].

Compared to impacts, blasting loads are more frequent encountered in rock engineering, and therefore, the corresponding study is more significant. Blasting loads are more complicated than impacting loads mainly in two aspects: first the loading rate of blasting is higher than that of impacting, and second blast-induced waves are diverging spherical waves or cylindrical waves, whereas impact-induced waves by SHPB or drop weight systems are simple one dimensional P-wave. Therefore, the cracked material behavior under blasting loads may differ largely from that under impacting loads, thus it is impossible to use the studying results of material response under impacting loads instead of those under blasting loads.

By using dynamic caustics test system, mode I crack behavior and dynamic stress intensity factors of PMMA under blasting loads were investigated [17–19], and the results showed that in the early stage of crack propagation, generally the crack belongs to model I, and tensile fracture characteristics can be observed from the crack surfaces. However, in the final stage of propagation, the crack belongs to I/II mixed mode, and both tensile and shear fracture characteristics can be observed. Zhu et al. [20] and Xu et al. [21] conducted blasting experiments by using detonators and cement mortar rectangle specimens with a mode-I crack, and the initiation toughness of cement mortar was determined through experimental-numerical method. Li et al., [22,23] investigated the effect of empty holes on propagating cracks under blasting loads, and they pointed out that empty holes have the arrest function on outgoing cracks, and the arrest function depends on the two hole spacing. Trivino and Mohanty [24] conducted in-situ tests and the results showed that most damage was caused by the expansion of gases, while its magnitude and extension were strongly dependent on confining conditions along the blasthole.

Numerical simulation is an essential part in the study of rock fractures under blasting because it can be applied not only in the validation of blasting test results, but also in the prediction of material dynamic behavior under various conditions, which may not be able to realize in experiments. Therefore, considerable numerical simulations have been performed by using different numerical models and numerical techniques, such as Donze et al. [25] applied a discrete element model to investigate the initiation and propagation of radial cracks; Ma and An [26] applied LS-DYNA code to investigate the efficiency of two major blast control methods; Wang et al. [27] applied coupled numerical codes of LS-DYNA and UDEC to investigate blasting-induced spalling damage in a rock; Zhu et al. [28] proposed a coupled multiphysical model for the interaction between blasting damage of coal seam and gas flow; Chen and Zhao [29] applied UEDC code to simulate blasting wave propagation in joint rock mass. In addition, a finite difference code AUTODYN has been applied in the simulation of rock dynamic behavior under impacting loads [7,11,12] and blasting loads [30–33], and the simulation results of crack propagation paths agree well with the test results. In this study, AUTODYN code is applied in the simulation of crack propagation under blasting loads.

Although considerable effort, both from experimental and numerical points of view, has been devoted to the study of rock dynamic behavior under blasting, and many significant results have been achieved, there still remain a number of unanswered or partially unanswered aspects, such as the crack propagation behavior under blasting and the measuring method of critical dynamic SIFs of brittle materials under blasting, and these two aspects will be focused in this paper.

2. Experimental study

In this paper, blasting tests by using single internal crack circular disc (SICCD) specimens were conducted, and the dynamic propagation parameters are measured.

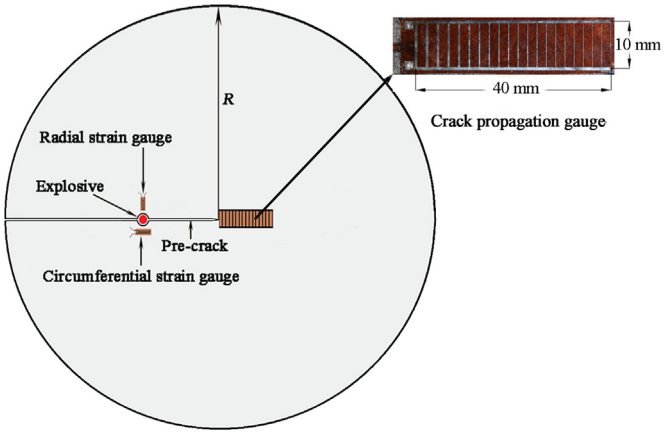

Fig. 1. Sketch of a SICCD specimen with a pre-crack, a borehole and a CPG stuck along crack propagation path.

2.1. SICCD specimen

In order to study crack dynamic propagation behavior under blasting loads, a single internal crack circular disc (SICCD) specimen as shown in Fig. 1 is proposed in this paper. The crack tip is located at the center of the circular specimen, and the borehole which is 7.0 mm in diameter is charged with a detonator which measures 7.0 mm in diameter. The radius of the circular specimen R is 250 mm, and the pre-crack length a is 100 mm.

As the detonator is fired, shock waves arise out of detonation in the borehole, and the high pressure on the borehole wall sets off shock waves in the adjacent rock mass, but it soon decays to high amplitude stress waves propagating at the speed of P- wave in the rock mass. Under the action of such dynamic stress waves, the crack will initiate and propagate, and the initiation time and the propagation time in different locations can be measured by the crack propagation gauge (CPG) which is stuck along the crack propagation path.

Green sandstone which is compact and uniform was selected to make the specimens. The experiment results [34,35] by using Polymethyl Methacrylate (PMMA) showed that the fracture characteristics under dynamic loads are similar to those observed in the homogeneous rocks. In addition, PMMA has the property of uniformity, high density and good transparency, thus crack propagation behavior induced by blasting can be observed easily. Therefore, except for sandstone, PMMA material ($C_5H_8O_2$) was also applied in this study. The P-wave and S-wave speeds of the sandstone and PMMA were measured by SonicViewer-SX device, and according to the P-wave and S-wave speeds, the dynamic elastic modulus and the dynamic Poisson's ratio of the sandstone and PMMA were obtained, and the results are presented in Table 1.

2.2. Measuring system

In the blasting tests, a data acquisition system was applied which consists of a CS-1D ultra-dynamic strain amplifier with 10 MHz sampling frequency and a DS1104 oscilloscope, as shown in Fig. 2. The crack initiation time, propagation time and propagation speeds were measured by crack propagation gauges (CPGs) which consists of 25 fine wires, as shown in Figs. 1 and 2. The total length of the CPGs is 40 mm, and the width is 10 mm, and the distance between two adjacent wires is 1.67 mm. The CPG was stuck along crack propagation path, and it connected with resistor R_1 (50 Ω) in parallel, and connected with resistor R_2 (50 Ω) in series, which can output a constant voltage during the tests.

The CPGs was stuck evenly to ensure that there is no air in the contact surface. When the crack starts to propagate, the wires of the

Table 1
Dynamic parameters of PMMA and sandstone.

parameters	P-wave speed C_p /(m/s)	S-wave speed C_s /(m/s)	Elastic modulus E_d /(G N/m^2)	Poisson's ratio ν_d	Density ρ /(Kg/m^3)
PMMA	2160	1450	6.1	0.31	1180
Sandstone	2430	1260	12.5	0.26	2370

CPG will break one by one, and a ladder-shaped voltage signal can be measured. The first wire of the CPG must coincide with the crack tip, and the breaking time of the first wire is the crack initiation time.

2.3. Rationality of SICCD specimen dimensions

Ravi-chandar and Knauss 13 investigated crack propagation behavior on Homalite 100 under stress wave loads, and they pointed out that stress wave reflection may exists in the boundary as using relatively small specimens, and the deviation of crack propagation caused by reflected waves cannot be ignored. Therefore, specimen dimensions in blasting experiments should be large enough so to avoid the effect of reflected tensile stress waves on crack propagation behavior. The threshold value of specimen dimensions can be determined according to the method that as reflected tensile waves from specimen boundaries reach crack tips, the crack propagation activity should have completed. Apparently in this case, the effect of the reflected tensile stress waves can be ignored.

In order to exam the rationality of the specimen dimensions, blasting experiments were first conducted by using the SICCD specimens of the sandstone and PMMA, and the test results are presented in Fig. 3. The shortest distance of the reflected waves to the crack tip is along the path from the borehole to the left side of the specimen and return to the moving crack tip.

The P-wave speed of sandstone is 2430 m/s, and the distance from the borehole center to the left boundary L was 150 mm, and the radius R of the specimen was 250 mm, and the crack propagated length was 40 mm. The shortest time as the reflected tensile stress waves reached the crack tip can be calculated by $(L + R + 40) / 2430$ mm/ms, and the result is 181.07 μs. For the sandstone specimen, the test results by the CPG show that the crack was completely stopped at the time 137.8 μs which is less than 181.07 μs, that means as the reflected tensile stress waves reached the crack tip, the crack propagation activity has stopped for 43.27 μs. Therefore, the sandstone specimen dimension in this study is large enough, and the crack dynamic behavior was not affected by the reflected tensile stress waves.

For the PMMA specimen, the crack has reached the edge of the SICCD specimen, and the CPG length was only 40 mm. Therefore, we only study the crack dynamic behavior in the range from the initiation to the end of the CPG in this study. Similarly, the shortest time as the reflected tensile stress waves reached the crack tip can be calculated by $(L + R + 40) / 2160$ mm/ms, and the result is 203.7 μs, whereas the test results show that the last wire of the CPG was broken at the time 171.44 μs, which means that as the reflected tensile waves reached the last wire of the CPG, the crack has left there for 58.5 μs. Therefore, the reflected tensile stress wave did not affect the crack propagation behavior, and both the dimensions of the PMMA and the sandstone specimens are large enough and applicable.

2.4. Measurement of blast-induced pressures

In order to measure crack initiation and propagation time as well as the propagation speeds, a CPG was stuck along the crack propagation path, as shown in Fig. 4. The thickness of the specimen was 15 mm and the borehole was charged with a detonator, and the part of the base charge of detonators was placed inside the specimens. No coupling and no stemming were applied in the blast tests, and a circular rubber ring was used to fix the detonator, as shown in Fig. 4.

The preliminary test results show that for the sandstone SICCD specimen charged with a detonator, the radius of the blast-induced crushed zone is less than 25 mm. Therefore, in order to measure the blast-induced strains around the borehole which can be used to calculate the pressure around the borehole, two strain gauges were stuck in the place 30 mm away from the borehole center, and one was stuck radially and the other was stuck circumferentially, as shown in Fig. 4.

By using the above test system, the voltage signal can be measured, and the voltage signal can be converted into strains by Eq. (1)

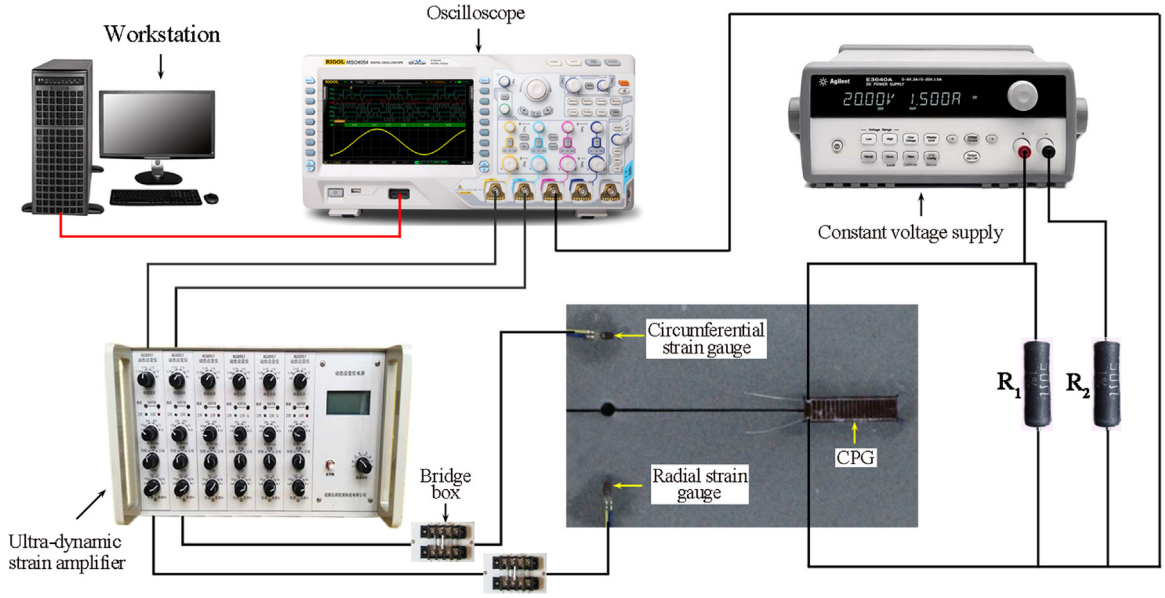

Fig. 2. The test system applied in the blasting tests.

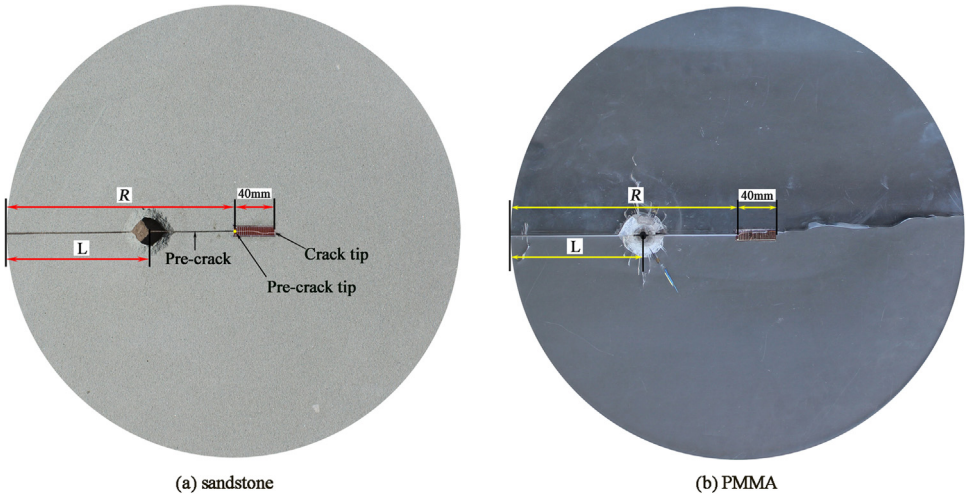

Fig. 3. Test results of SICCD specimens of sandstone and PMMA under blasting.

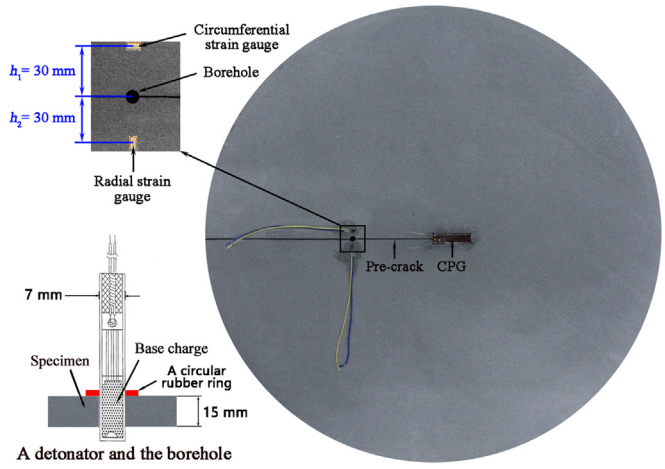

Fig. 4. A SICCD specimen with two strain gauges, a CPG and a detonator charged in the borehole.

$$\varepsilon = \frac{4\Delta U}{nEK} \tag{1}$$

where ε is strain, ΔU is the measured voltage, n is amplification of dynamic strain gauge ($n = 1000$), E is the bridge box voltage ($E = 2\ V$), and K is sensitivity coefficient of strain gauge ($K = 2.1$).

Let ε_c and ε_r represent the circumferential strain and the radial strain measured by the circumferential strain gauge and the radial strain gauge, respectively, and the test results of the two strains as a function of time are shown in Fig. 5. It can be seen that the peak (absolute) value of the circumferential tensile strain is larger than that of the radial compressive strain, but the time corresponding to the peak value of the circumferential strain is later than that of the radial strain.

According to the stress-strain relationship for plane stress problems, the blast-induced compressive stresses can be calculated by

$$p(t) = \frac{E_d}{1 - \nu_d^2}(\varepsilon_r(t) + \nu_d \cdot \varepsilon_c(t)) \tag{2}$$

where $p(t)$ is the pressure acting on the place 30 mm away from the borehole center (see Fig. 4), E_d is the dynamic elastic modulus, ν_d is dynamic Poisson's ratio. According to the curves of strains versus time shown in Fig. 5, the pressures can be calculated by using Eq. (2), and the curve of pressures versus time for sandstone specimen #6 is presented in Fig. 6.

The peak value for the sandstone specimen under blasting was 62.9 MPa in Fig. 6. For typical commercial explosives, the detonation pressure exerted on the borehole wall at the moment of initiation could easily exceed 10 GPa [2], but in this study, only a detonator was applied, and the two strain gauges were stuck at the place 30 mm away from the borehole center. Therefore, the pressure measured in these tests was comparatively low.

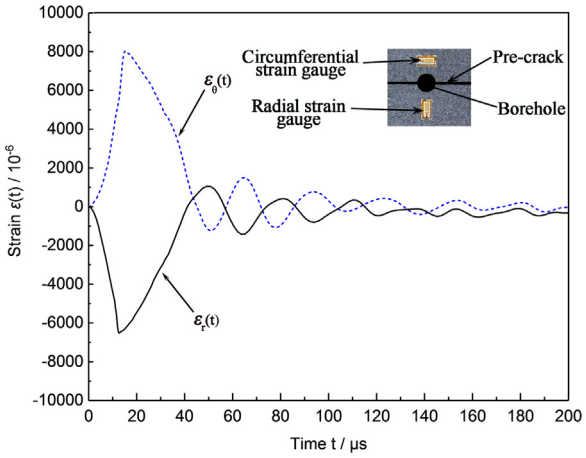

Fig. 5. The curves of strains versus time measured by the two strain gauges stuck in the place 30 mm away from the borehole center.

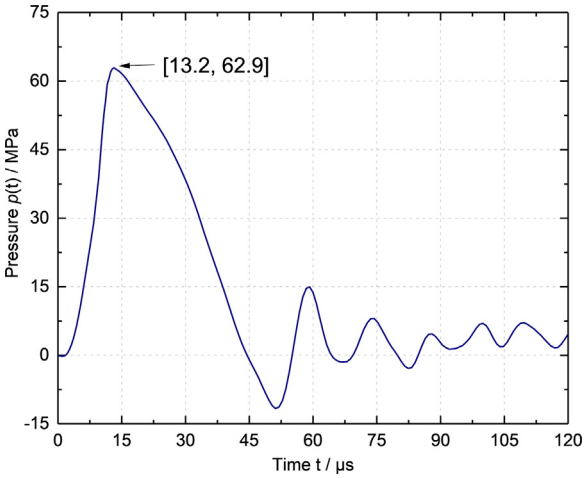

Fig. 6. The curve of blast-induced pressures versus time measured by the two strain gauges stuck in the place 30 mm away from the borehole center.

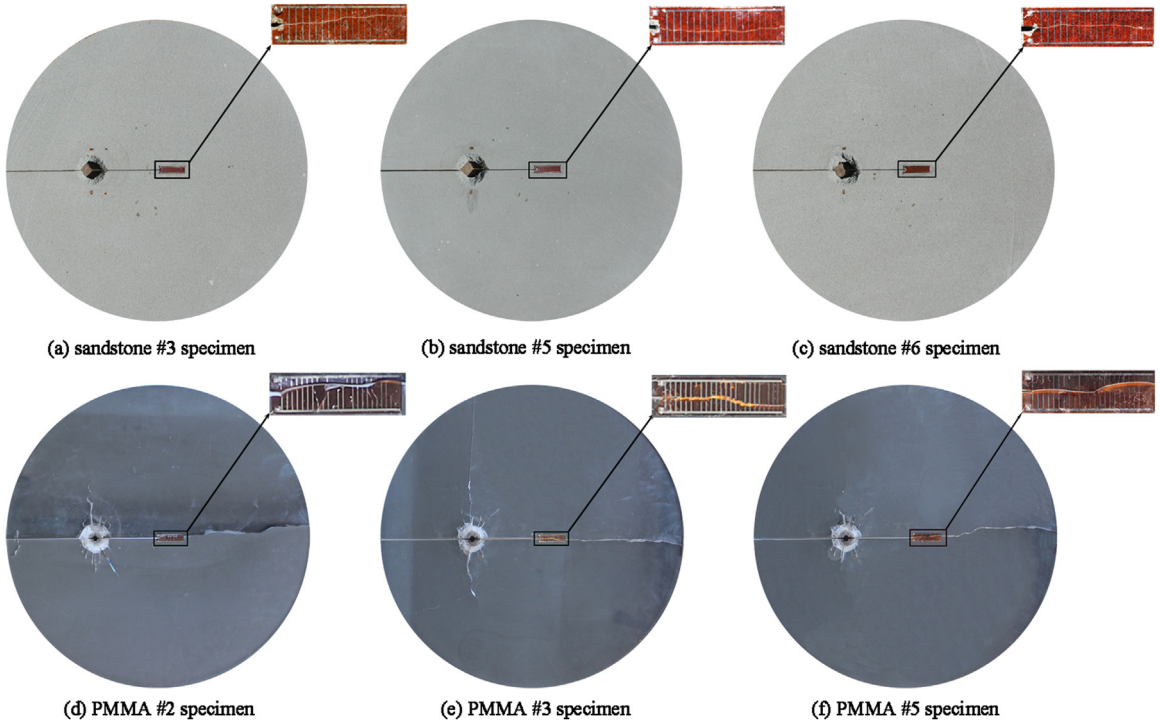

Fig. 7. The fracture patterns of three sandstone specimens and three PMMA specimens after blasting.

2.5. Crack propagation path

After initiations, the blast-induced shock waves first exerted on the borehole wall and the rock mass was seriously damaged around the borehole. This damaged zone is called crushed zone, and the radius of the crushed zone is about 22.6–23.7 mm for sandstone, and 23–25 mm for PMMA. The strain gauges were thus stuck in the place 30 mm away from the borehole center. The crack propagation paths of three sandstone specimens and three PMMA specimens after blasting are presented in Fig. 7.

From Fig. 7, one can find that the propagation path is not a straight line. This may be caused by the heterogeneous property of sandstone and PMMA materials and the dynamic energy release rate may not be a constant. In addition, the boreholes were artificially conducted and they may be not exactly a normal circle, which could lead to imbalanced stress waves near the crack tips, and therefore, the crack could deviate from the original propagation path, but the deviation is small.

2.6. Crack propagation speeds and propagation time

The CPG consists of 21 wires or 25 wires, and as the crack starts to propagation, the CPG wires will be broken one by one, and a ladder-shaped curve of voltage signal versus time can be measured. For a sandstone specimen #6, the measurement results are shown in Fig. 8(a). The crack propagation speeds can be calculated according to the wire interval distance and the wire broken time, and the results are shown in Fig. 8(b) for three sandstone specimens and 8(c) for three PMMA specimens.

From Fig. 8(b) and (c), one can find that the crack propagation speed is not a constant. For sandstone specimen #6 shown in Fig. 8(a), between the 4th wire and the 6th wire, the crack propagation speed is only about 189.2 m/s, whereas around the 15th wire, the crack speed is 876.31 m/s which is 3.6 times that between the 4th and 6th wire. At the 21th wire, the crack speed is very low, and just behand the 21th wire, the crack is fully stopped. Fig. 8(d) shows the average crack propagation speeds of the tested specimens. The average propagation speed for all the sandstone specimens is 415.16 m/s and for all the PMMA specimens it is 364.27 m/s. One may conclude that the average crack propagation speed of sandstone is larger than that of PMMA under the same dynamic loadings, and crack propagation speed is related to the material wave impedance.

The crack propagation speeds and propagation time will be applied in the subsequent calculation of the initiation toughness and the propagation toughness.

3. Numerical simulation

In order to simulate crack propagation behavior under blasting, finite difference code AUTODYN was employed in this numerical study. AUTODYN code has been applied widely in solving dynamic problems, and its effectiveness has been well validated [2,8,30–32].

3.1. Numerical models

Finite difference models of the SICCD specimen under blasting were established by using AUTODYN code in this paper. Two-dimensional quadrilateral elements were applied in the discretization of SICCD specimens, and the total element number was 388574, as shown in Fig. 9. Since no stemming and no coupling were applied to the borehole, the blast-induced gas products would leak out, that means the gas products did not play any role in the crack propagation. Only the shock wave action in this numerical study was simulated. The material parameters of PMMA and sandstone are presented in Table 1. The crack width was 1.0 mm, and the length was 100 mm for the sandstone models and the PMMA models.

In the numerical model, the crack tip was 100 mm away from the borehole. As the stress wave reached the crack tip, it was decayed to elastic stress wave. Because both the pressure and deformation are relatively small at the crack tip, and the blasting near the borehole was not the focus of this study, linear equation of state (EOS), which assumes that the pressure and energy are irrelevant, was applied to the PMMA and sandstone models. The linear EOS can be written as

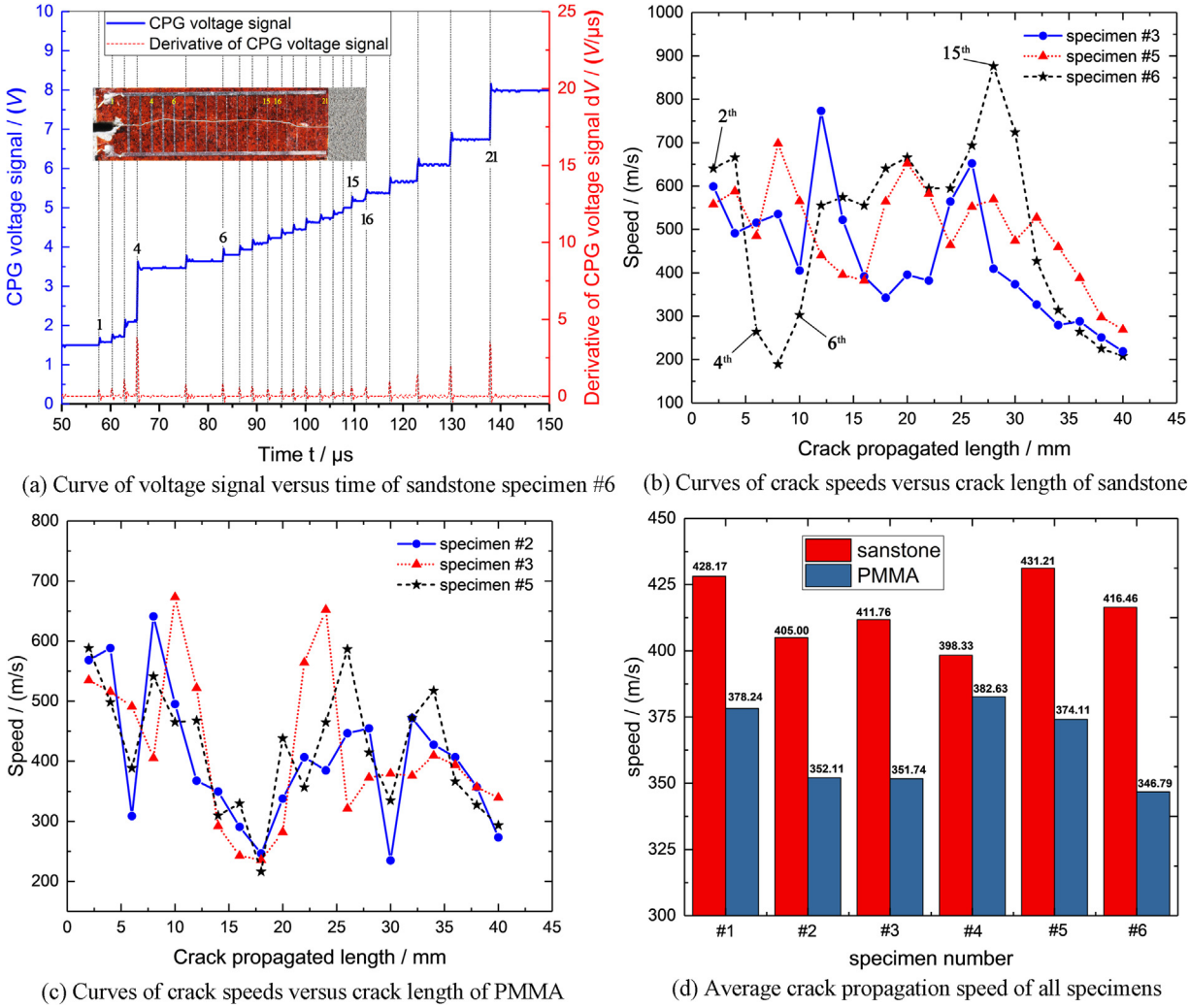

(a) Curve of voltage signal versus time of sandstone specimen #6

(b) Curves of crack speeds versus crack length of sandstone

(c) Curves of crack speeds versus crack length of PMMA

(d) Average crack propagation speed of all specimens

Fig. 8. The voltage signal and the corresponding crack propagation speed.

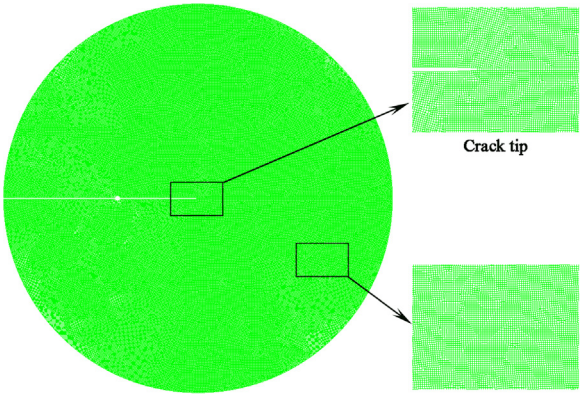

Fig. 9. Mesh of a SICCD specimen.

$$P(\rho) = \kappa\left(\frac{\rho}{\rho_o} - 1\right) \tag{3}$$

where κ is bulk modulus, ρ_0 and ρ are the density in initial state and in current state, respectively.

For the Hexogen explosive of the detonator, Jones-Wilkins-Lee (JWL) EOS was applied. The JWL EOS is especially suited for hydrodynamic of explosive detonation products, and it is widely applied in the numerical simulation of explosive explosion [2,22,23,30,32,33]. It was employed as the EOS of the Hexogen explosive in this study, and it can be expressed as

$$P = A\cdot\left(1-\frac{\omega}{R_1 V}\right)\cdot e^{-R_1 \upsilon} + B\cdot\left(1-\frac{\omega}{R_2 V}\right)\cdot e^{-R_2 \upsilon} + \frac{\omega E_0}{V} \tag{4}$$

where P is the pressure, E_0 is the total initial energy, V is the specific volume of detonation products, and A, B, R_1, R_2 and ω are constants, and $A = 778.3$ GPa, $B = 7.071$ GPa, $R_1 = 4.2$, $R_2 = 1.0$, $\omega = 0.03$. These parameters have been well validated [22,23,32,33].

For the rock specimen, the major principal stress and the maximum shear stress failure criterion were applied in describing the material status, which means that when the major principal stress σ_1 of an element reaches the dynamic tensile strength σ_T or the maximum shear stress τ_{max} reaches the dynamic shear strength of the material τ_c, then the element is failed, i.e.

$$\sigma_1 \le \sigma_T \text{ or } \tau_{max} \le \tau_c \tag{5}$$

3.2. Numerical simulation results

The numerical simulation by the models established by using the above EOS and failure criterion was carried out, and the simulation results of one sandstone mode and one PMMA model are presented in Fig. 10. Since both the sandstone and PMMA are brittle materials, the fracture mechanism of them are similar. In order to investigate the fracture mechanism, a group of gauge points were designed along the

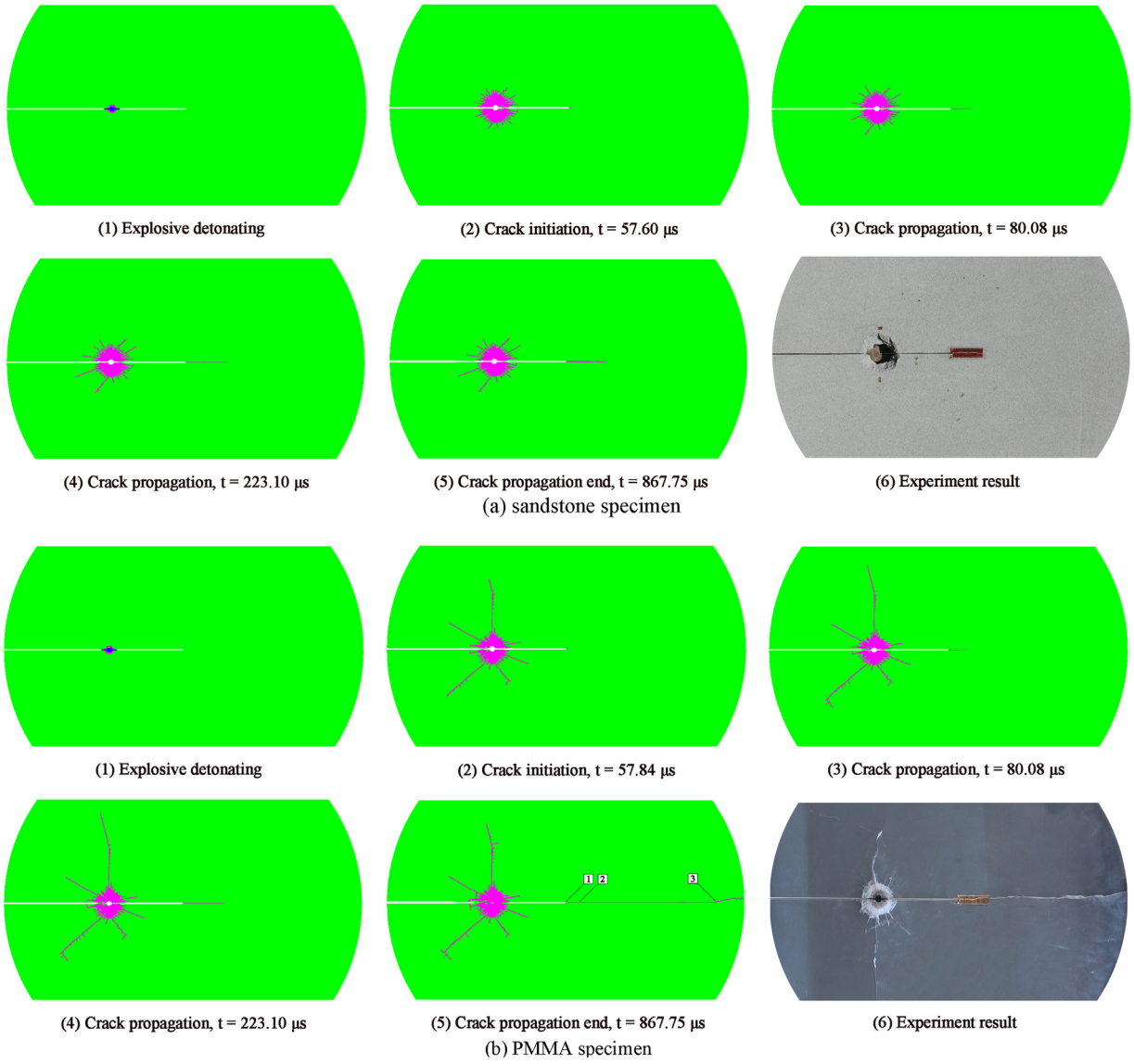

Fig. 10. The simulation results of crack propagation path as a function of time. (a) (b).

crack propagation path in PMMA, as shown in Fig. 10(b), and the stresses at gauge points 1, 2 and 3 are presented in Fig. 11.

The simulation results show that the crack propagation path at the early stage is a straight line, but at gauge point 3 which is near the free boundary, it starts to curve, as shown in Fig. 10(b). The simulation results generally agree with the test results, and the slight difference may be caused by the heterogeneous property of sandstone and PMMA materials.

Gauge point 1 was designed at the crack tip, and the stress σ_x, σ_y and τ_{xy} as a function of time are presented in Fig. 11(a). The peak value of stress σ_y is 30.21 MPa which is larger than the tensile strength 30 MPa of PMMA, thus the crack is initiated.

For gauge point 2, the stresses σ_x, σ_y and τ_{xy} are presented in Fig. 11(b). The normal stress σ_y at the time 80.08 μs reaches 30.29 MPa which is larger than the tensile strength of the PMMA, thus the element at point 2 is also failed, and the crack propagates through point 2 under the normal stress σ_y.

For gauge point 3, the stresses σ_1, σ_y and τ_{xy} are presented in Fig. 11(c). One can find that the peak value of the stress σ_y is 19.58 MPa which is less than the PMMA tensile strength, whereas the major principal stress σ_1 is 30.01 MPa which is larger than the PMMA tensile strength. The angle between the major principal stress and the horizontal axis is 14.23°, and therefore, the crack path starts to curve at the gauge point 3, as shown in Fig. 11.

4. Critical dynamic SIFs

Critical dynamic SIFs are a threshold value applied in the prediction of crack status. For brittle materials under impact loads, the fracture behavior has been well studied by many researchers [9–12,36,37], but for those under blasting loads, less attention has been paid.

4.1. Calculation of dynamic SIFs by ABAQUS code

Although AUTODYN code may be applied in the calculation of stress intensity factors (SIFs), the effectiveness has not been well validated, whereas ABAQUS code has been applied widely in the calculation of SIFs. Therefore, ABAQUS code was applied in this study, and finite element models for the sandstone and PMMA SICCD specimens under blasting were established. The region near crack tip was meshed by using quarter-point triangular elements CPS6, as shown in Fig. 12, and for other region, quadrilateral elements CPS8 were applied.

Because the pressure shown in Fig. 6 was measured in the location 30 mm away from the borehole center, in the finite element models, the

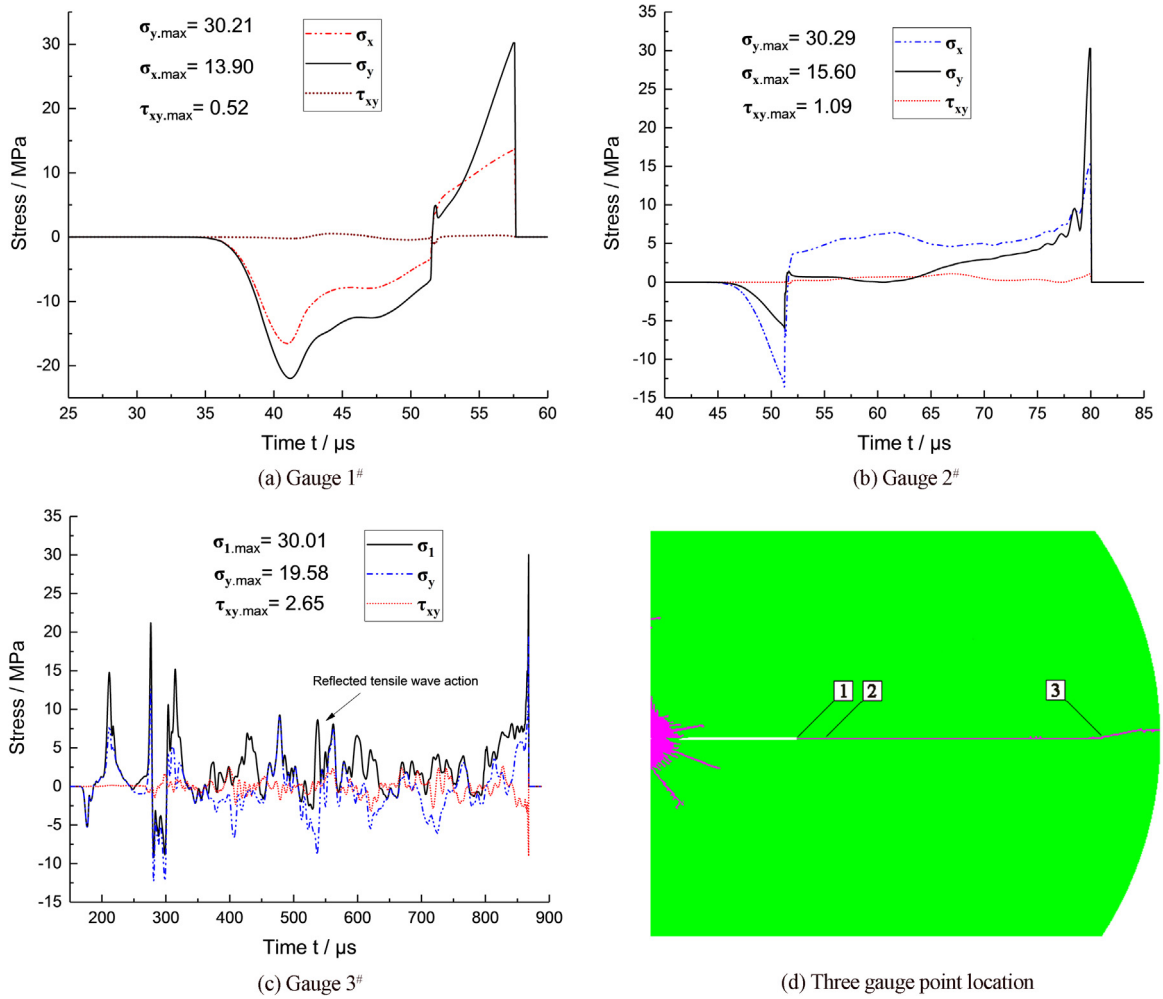

Fig. 11. The curves of stresses versus time at three gauge points.

borehole diameter was enlarged to 60 mm which is much larger than the original borehole diameter 7 mm, and the loading curve shown in Fig. 6 was applied on the hole wall of the models. The crack was considered as an ideal sharp crack, and the mesh near the crack was refined in order to calculate precise SIFs. According to the theory of fracture mechanics, the SIF $K_I(t)$ can be calculated according to the displacement at point A and B in Fig. 12, and it can be expressed as [11,12]

$$K_I(t) = \frac{E}{24(1-\nu^2)}\sqrt{\frac{2\pi}{r_{OA}}}\,[8v_A(t) - v_B(t)] \tag{6}$$

where $r_{OB} = 4r_{OA}$, and $v_A(t)$ and $v_B(t)$ are the displacements in y

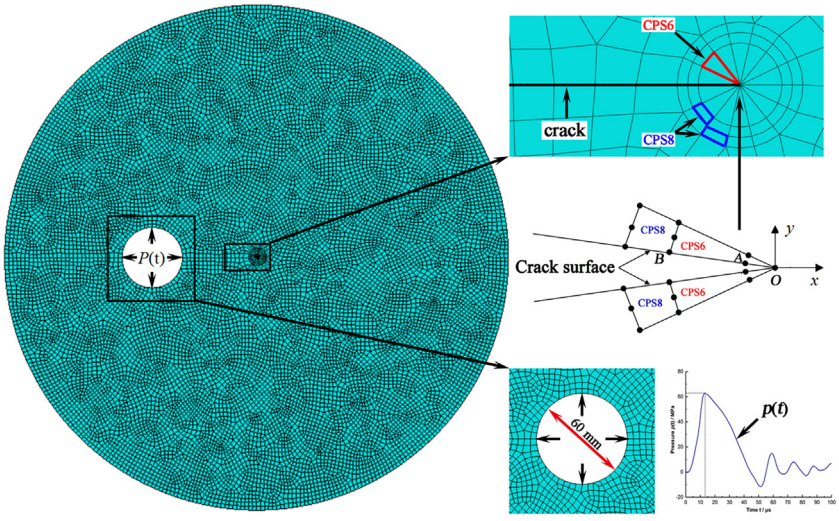

Fig. 12. Mesh of a SICCD specimen applied in the calculation of dynamic SIFs by using ABAQUS code.

direction at point A and B, respectively, E is elastic modulus, ν is Poisson's rate, and r_{OA} is the distance from point O to A.

4.2. Dynamic SIFs of moving cracks

For a moving crack, the dynamic SIF is different from those of stationary cracks. The dynamic SIF $K_I^d(t)$ should be the product of the SIF $K_I^0(t)$ of the stationary crack and the universal function $k(v)$ [38,39], i.e.

$$K_I^d(t) = k(v)\cdot K_I^0(t) \tag{7}$$

where v is the instantaneous crack velocity, and $k(v)$ is universal function, and it can be approximated as [39]

$$k(v) = \frac{1 - v/C_R}{\sqrt{1 - hv}} \tag{8}$$

where the factor $h = \frac{2}{C_p}\left(\frac{C_s}{C_R}\right)^2\left(1 - \frac{C_s}{C_p}\right)^2$, C_p is P-wave speed, C_R is Rayleigh wave speed and C_s is S-wave speed. Obviously, as $v = 0$, then $k(0) = 1$, that means for the cracks in the state of initiation and arrest, the universal function equals to 1.0, and the corresponding dynamic SIFs don't need to times the universal function. When $v = C_R$, $k(C_R) = 0$, that means as cracks propagate with Rayleigh wave speed, the dynamic SIFs equal to zero.

4.3. Critical dynamic SIFs in initiation and in propagation

The sandstone specimen #6 is selected as an example to illustrate the procedure of the determination of the critical dynamic SIF in initiation and in propagation.

For the crack at initiation, the crack propagation speed v is 0. According to the crack length and the loading curve as shown in Fig. 6 measured in the blasting tests, the numerical model was established by using ABAQUS code, and the crack dynamic SIFs were calculated. The results of crack dynamic SIFs as a function of time are presented in Fig. 13(a). It can be seen that the dynamic SIFs vary with time, and at the early stage, as the stress wave just reaches the crack tip, the SIF is negative under compression, and then the SIFs start to increase. The test results show that the crack was initiated at the time 57.6 μs, then the value 2.83 MPa $\sqrt{m}$ in the vertical axis which corresponds to 57.6 μs in the horizontal axis is the critical SIF which could be considered as the initiation toughness of the sandstone.

As the propagating crack reached the 5th wire of the CPG, the crack length was 106.67 mm, and the dynamic SIFs can be calculated according to the crack dimensions and the loading curve as shown in Fig. 6. The calculation results of the dynamic SIFs $K_I^0(t)$ as a function of time are presented in Fig. 13(b) (the dashed curve). The crack propagation speed was 189.2 m/s at the 5th wire, and then the universal function $k(v)$ can be calculated by Eq. (8), and the dynamic SIF $K_I^d(t)$ can be calculated by Eq. (7). The curve of the dynamic SIFs $K_I^d(t)$ versus time is presented in Fig. 13(b) (the solid curve). The test results show that the 5th wire was broken at the time 75.4 μs, and then the critical dynamic SIF 2.11 MPa $\sqrt{m}$ in the vertical axis can be determined from Fig. 13(b). This critical dynamic SIF could be considered as the propagation toughness.

The test results of the sandstone specimen #6 (in Fig. 8) show that the crack fully stopped between the 21th wire and the 22th wire, but the exact arrest time cannot be determined.

Similarly, the propagation toughness at the other wire places of sandstone specimen #6 can be obtained, and for all the sandstone and PMMA specimens, the crack propagation speeds and the propagation toughness at all the wire places can be obtained. The relationship between the propagation toughness and crack propagation speeds are presented in Fig. 14. It can be seen that the propagation toughness for both sandstone and PMMA generally decreases with the increase of crack propagation speeds. This can be explained that as crack speeds increase, the dynamic SIFs decrease according to Eqs. (7) and (8).

4.4. Dynamic energy release rate

The dynamic energy release rate is defined as the rate of mechanical energy flow out of the body and into the crack tip per unit crack advance. Freund analyzed the relation between the dynamic energy release rate and dynamic SIFs, which, in plane stress, can be expressed as [40]

$$G = \frac{1}{E_d}[A_I(v)\bullet K_I^2 + A_{II}(v)\bullet K_{II}^2] \tag{9}$$

where $A_I(v)$ and $A_{II}(v)$ are the universal functions related to the crack propagation speed, and v is the crack propagation speed as the speeds shown in Fig. 8(b), (c), when $v = 0$, $A_I(v) = A_{II}(v) = 1$; when $v \neq 0$, $A_I(v) = v^2\bullet a_d/((1-\nu_d)\bullet C_s^2\bullet D)$, $A_{II}(v) = v^2\bullet a_s/((1-\nu_d)\bullet C_s^2\bullet D)$, $D = 4a_s\bullet a_d - (1+a_s^2)^2$, $a_d = \sqrt{1-v^2/C_d^2}$, $a_s = \sqrt{1-v^2/C_s^2}$; E_d is the dynamic elastic modulus of material, C_p is the P-wave speed, C_s is the S-wave speed and ν_d is the dynamic Poisson's ratio.

The dynamic energy release rate at the crack tip versus crack propagated length can be calculated by Eq. (9), and the results are presented in Fig. 15. The dynamic energy release rate at the crack tips of the sandstone and PMMA specimens is not constant which may be able to explain the non-straight propagation paths shown in Fig. 7. The release rate first decreases with the increase of crack propagated length. As the extended length is about 14 mm for the sandstone and 18 mm for the PMMA, the release rate is the minimum. After the minimum, the

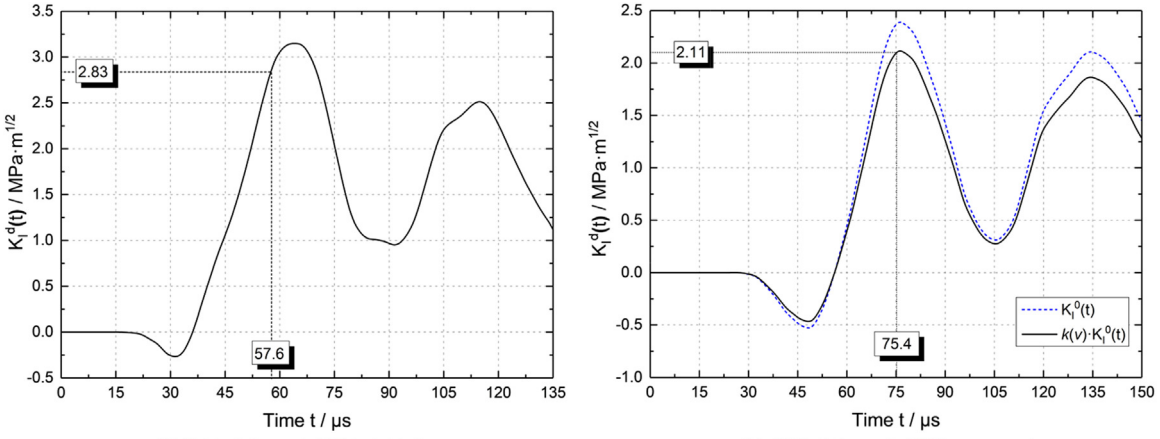

(a) Critical dynamic SIF in initiation (b) Critical dynamic SIF in propagation

Fig. 13. Determination of the critical dynamic SIFs in initiation and in propagation of sandstone specimen #6.

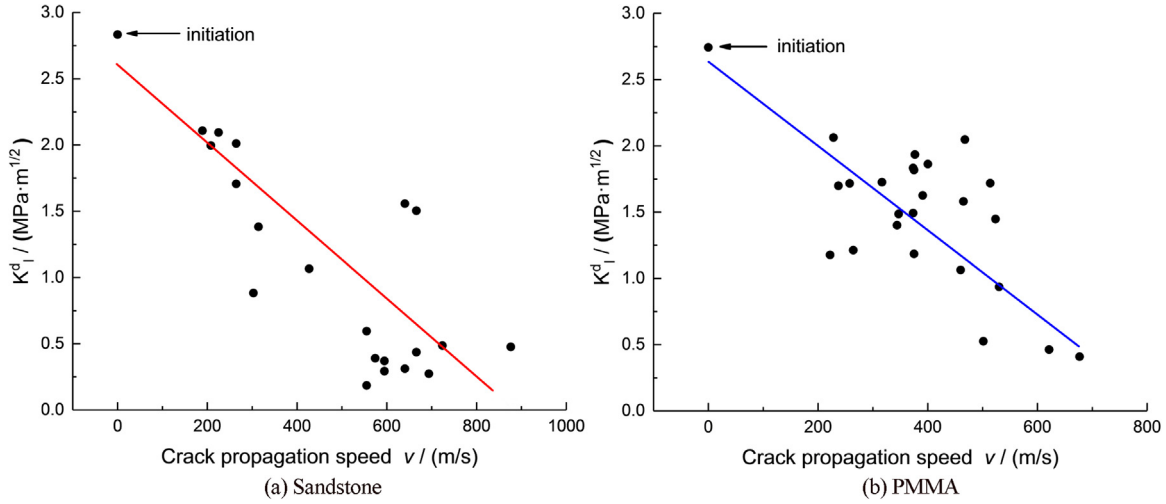

Fig. 14. The test results of the dynamic toughness versus crack propagation speed of sandstone and PMMA.

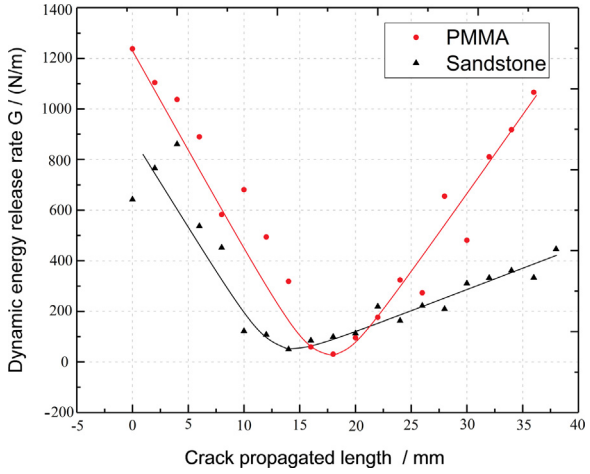

Fig. 15. The test results of the dynamic energy release rate versus crack propagated length of sandstone and PMMA.

release rate starts to increase with the crack propagated length, but the release rate of PMMA rises more sharply than that of the sandstone.

5. Conclusions

(1) A new method of measuring model I initiation toughness and propagation toughness of brittle materials under blasting loads is proposed. Experimental - numerical method can be applied in the determination of the critical dynamic SIFs in crack initiation and in propagation.
(2) A new configuration specimen, i.e. single internal crack circular disc (SICCD), is proposed in this paper, and the SICCD specimens as well as crack propagation gauges (CPGs) have been applied in the blasting experiments.
(3) In blasting experiments, the specimen dimensions must be large enough, and the threshold dimension of specimens can be determined according to the method that as the reflected tensile waves reach the crack tip, the crack propagation activity have completed.
(4) For mode I crack under blasting loads, the crack propagation speeds are not constants; the crack speeds in sandstone are larger than those in PMMA under the same conditions; the propagation toughness decreases with the increase of crack propagation speeds.

Acknowledgements

This work was financially supported by the National Natural Science Foundation of China (11672194; 11702181), by Sichuan Administration of Work Safety (aj20170515161307) and by the project of Department of Science and Technology of Sichuan Province (2018JZ0036).

References

[1] Dong ZX, Liu G. Roadway engineering. China University of Mining and Technology Press; 2013. p. 84–98.
[2] Zhu ZM, Mohanty B, Xie HP. Numerical investigation of blasting-induced crack initiation and propagation in rocks. Int J Rock Mech Min Sci 2007;44(3):412–24.
[3] Hu R, Zhu ZM, Hu ZY. Experimental study of regularity of crack propagation under blasting dynamic loads. Chin J Rock Mech Eng 2013;32(7):1476–81.
[4] Zhang QB, Zhao J. Determination of mechanical properties and full-field strain measurements of rock material under dynamic loads. Int J Rock Mech Min Sci 2013;60(8):423–39.
[5] Zhang QB, Zhao J. Effect of loading rate on fracture toughness and failure micromechanisms in marble. Eng Fract Mech 2013;102(2):288–309.
[6] Wang QZ, Feng F, Ni M, Gou XP. Measurement of mode I and mode II rock dynamic fracture toughness with cracked straight through flattened Brazilian disc impacted by split Hopkinson pressure bar. Eng Fract Mech 2011;78(12):2455–69.
[7] Wang M, Zhu ZM, Dong YQ, Zhou L. Study of mixed-mode I/II fractures using single cleavage semicircle compression specimens under impacting loads. Eng Fract Mech 2017;177:33–4.
[8] Wang M, Zhu ZM, Wang X. The growth of mixed-mode I/II crack under impacting loads. Chin J Rock Mech Eng 2016;35(7):1323–32. https://doi.org/10.13722/j.cnki.jrme.2015.1260. [in Chinese].
[9] Yang JR, Zhang CG, Zhou Y, Zhu ZM, Wang QZ. A new method for determing dynamic fracture toughness of rock using SCDC specimens. Chin J Rock Mech Eng 2015;34(2):279–92. https://doi.org/10.13722/j.cnki.jrme.2015.02.007. [in Chinese].
[10] Ni M, Gou XP, Wang QZ. Test method for rock dynamic fracture toughness using single cleavage drilled compression specimen impacted by split Hopkinson pressure bar. Eng Mech 2013;30(1):365–71.
[11] Wang XM, Zhu ZM, Wang M, Ying P, Zhou L, Dong YQ. Study of rock dynamic fracture toughness by using VB-SCSC specimens under medium-low speed impacts. Eng Fract Mech 2013;181:52–64.
[12] Zhou L, Zhu ZM, Wang M, Ying P, Dong YQ. Dynamic propagation behavior of cracks emanating from tunnel edges under impact loads. Soil Dyn Earthq Eng 2018;105:119–26.
[13] Ravi-chandar K, Knauss WG. An experimental investigation into dynamic fracture: i. crack initiation and arrest. Int J. Fract. 1984;25(4):247–62.
[14] Zhou L, Zhu ZM, Dong YQ, Ying P. Dynamic response of cracks in tunnels under impact loading of medium-low speed. Chin J Rock Mech Eng 2017;36(6):1363–72. https://doi.org/10.13722/j.cnki.jrme.2016.1403. [in Chinese].
[15] Wang XM, Zhu ZM, Shi ZB, Fan Y, Kang JM. A method measuring dynamic fracture toughness of rock using VB-SCSC specimens. Chin J Rock Mech Eng 2018;37(2):302–11. https://doi.org/10.13722/j.cnki.jrme.2017.0351. [in Chinese].
[16] Ying P, Zhu ZM, Zhou L, Dong YQ, Wang X. Dynamic toughness of mode I crack under medium and low speed impacts. J China Coal Soc 2017;42(S2):338–45. https://doi.org/10.13225/j.cnki.jccs.2017.0058. [in Chinese].
[17] Li Q, Yang RS, Li JL. Experimental study on propagation of dynamic cracks under

blasting loading. Chin J Rock Mech Eng 2005;24(16):2912–6.
[18] Yang RS, Ding XC, Wang YB, Chen C. Action-effect study of medium under loading of explosion stress wave and explosion gas. Chin J Rock Mech Eng 2016;35(a02):3501–6. https://doi.org/10.13722/j.cnki.jrme.2016.0066. [in Chinese].
[19] Yue ZW, Yang RS, Guo DM, Cao H, Dong JC. Dynamic analysis of crack propagation in media containing flaws under the explosive stress wave. Rock Soil Mech 2009;30(4):949–54. https://doi.org/10.16285/j.rsm.2009.04.004. [in Chinese].
[20] Zhu ZM, Xu WT, Feng RQ. A new method for measuring mode-I dynamic fracture toughness of rock under blasting loads. Exp Tech 2015;40(3):899–905.
[21] Xu WT, Zhu ZM, Zeng LG. Testing method study of mode-I dynamic fracture toughness under blasting loads. Chin J Rock Mech Eng 2015;34(S1):2767–72. https://doi.org/10.13722/j.cnki.jrme.2014.0125. [in Chinese].
[22] Li M, Zhu ZM, Liu RF, Liu B, Zhou L, Dong YQ. Study of the effect of empty holes on propagating cracks under blasting loads. Int J Rock Mech Min Sci 2018;103:186–94.
[23] Li M, Zhu ZM, Xiao DJ, Hu R, Shi ZB. Mechanism of crack arrest by peripheral holes during mine rock roadway excavation under blasting. J China Coal Soc 2017;42(7):1691–9. https://doi.org/10.13225/j.cnki.jccs.2016.1226. [in Chinese].
[24] Trivino LF, Mohanty B. Assessment of crack initiation and propagation in rock from explosion-induced stress waves and gas expansion by cross-hole seismometry and FEM–DEM method. Int J Rock Mech Min Sci 2015;77:287–99.
[25] Donze FV, Bouchez J, Magnier SA. Modeling fractures in rock blasting. Int J Rock Mech Min Sci 1997;34(8):1153–63.
[26] Ma GM, An XM. Numerical simulation of blasting-induced rock fractures. Int J Rock Mech Min Sci 2008;45(6):966–75.
[27] Wang ZL, Li YC, Wang JG. Numerical analysis of blasting-induced wave propagation and spalling damage in a rock plate. Int J Rock Mech Min Sci 2008;45(4):600–8.
[28] Zhu WC, Wei CH, Li S, Wei J, Zhang MS. Numerical modeling on destress blasting in coal seam for enhancing gas drainage. Int J Rock Mech Min Sci 2013;59(5):179–90.
[29] Chen SG, Zhao J. A study of UDEC modelling for blast wave propagation in jointed rock masses. Int J Rock Mech Min Sci 1998;35(1):93–9.
[30] Zhu ZM, Xie HP, Mohanty B. Numerical investigation of blasting-induced damage in cylindrical rocks. Int J Rock Mech Min Sci 2008;45(2):111–21.
[31] Zhu Z, Wang C, Kang JM, Li YX, Wang M. Study on the mechanism of zonal disintegration around an excavation. Int J Rock Mech Min Sci 2014;67(4):88–95.
[32] Zhu ZM. Numerical prediction of crater blasting and bench blasting. Int J Rock Mech Min Sci 2009;46(6):1088–96.
[33] Zhu ZM, Li YX, Zhou ZR, Ran X, Jin XX. Dynamic response of defected rock under blasting load. Chin J Rock Mech Eng 2011;30(6):1157–67.
[34] Kutter HK, Fairhurst C. On the fracture process in blasting. Int J Rock Mech Min Sci 1971;8(3):181–202.
[35] Rossmanith HP, Daehnke A, Nasmillner REK, Kouzniak N, Ohtsu M, Uenishi K. Fracture mechanics applications to drilling and blasting. Fatigue Fract Eng Mater 1997;20(11):1617–36.
[36] Marshall GP, Williams JG, Turner CE. Fracture toughness and absorbed energy measurements in impact tests on brittle materials. J Mater Sci 1973;8(7):949–56.
[37] Weisbrod G, Rittel D. A method for dynamic fracture toughness determination using short beams. Int J Fract 2000;104(1):89–103.
[38] Rose LRF. Recent theoretical and experimental results on fast brittle fracture. Int J Fract 1976;12(6):799–813.
[39] Ravi-Chandar K. Dynamic fracture. Elsevier; 2004. p. 49–69.
[40] Freund LB. Dynamic fracture mechanics. Edinburgh: Cambridge University Press; 1990. p. 231–5.